

Combined hillslope and channel processes simulation applied to landscape and alluvial system modelling

Tristan Salles & Guillaume Duclaux

December 18, 2013

CSIRO Earth Science & Resource Engineering, 11 Julius Avenue North Ryde, NSW 2113, Australia

Abstract

We present a new numerical approach for simulating geomorphic and stratigraphic processes that combines open-channel flow with non-uniform sediment transport law, and semi-empirical diffusive mass wasting. It is designed to facilitate modelling of surface processes across multiple space and time scales, and under a variety of environmental and tectonic conditions. The physics of open-channel flow is primarily based on an adapted Lagrangian formulation of shallow-water equations. The interaction between flow and surface geology is performed by a non-uniform total-load sediment transport law. Additional hillslope processes are simulated using a semi empirical methods based on a diffusion approach. LECODE is the implementation of this combined approach. In this code, the resolution of flow dynamics is made on a triangulated grid automatically mapped and adaptively remeshed over a regular orthogonal stratigraphic mesh. These new methods reduce computational time while preserving stability and accuracy of the physical solutions. In order to illustrate the potential of this method for landscape and sedimentary system modelling, we present a set of three generic experiments focusing on assessing the influence of contrasting erodibilities on the evolution of an active bedrock landscape. The modelled ridges morphometrics satisfy established relationships for drainage network geometry and slope distribution, and provide quantitative information on the relative impact of hillslope and channel processes, sediment discharge, and alluviation. Our results suggest that contrasting erodibility can stimulate autogenic changes in erosion rate and influence the landscape morphology and preservation. The approach implemented in LECODE offers new opportunities to investigate joint landscape and sedimentary systems response to external perturbations. The possibility to define and track a large number of materials makes LECODE highly suitable to model source to sink problems where material dispersion is a key question that need to be addressed, such as alluvial exploration or basin analysis.

Keywords: Geomorphology; Stratigraphy; Ridge Formation; Contrasting Erodibility; Erosion rate.

1 Introduction

Understanding the evolution of the Earth's surface has been the challenging objective of geomorphologists and sedimentologists for over a century (*Gilbert*, 1895; *Davis*, 1899). The development of techniques such as geochronological techniques, remote sensing and geographic information systems (GIS) have made it possible to gather quantitative data and better constrain the evolution of the Earth's surface in a variety of environments. Modelling surface processes has allowed the geoscience community to test and develop new conceptual models and quantify the drivers

and feedback mechanisms responsible for shaping the Earth's surface (*e.g.*, *England and Molnar*, 1990; *Hasbargen and Paola*, 2000; *Bonnet and Crave*, 2003; *Paola et al.*, 2009). Over the past three decades, new numerical modelling methods have developed to address medium- to large-scale landscape evolution and stratigraphy reconstruction over spatial dimensions of a catchment to an orogen and temporal dimensions of 10^4 to 10^6 years (*e.g.*, *Koops*, 1989; *Kooi and Beaumont*, 1994; *Koops*, 1994; *Kooi and Beaumont*, 1996; *Dietrich et al.*, 2003; *Braun and van der Beek*, 2004; *Willgoose*, 2005; *Paola et al.*, 2009; *Tucker and Hancock*, 2010). While complex methods for simulating hydrodynamics and sediment transport exist, they are not well adapted to geological time scales. Diffusive models have been widely and successfully used to study geomorphic processes through geologic periods (*e.g.*, *Tucker and Slingerland*, 1994; *Howard et al.*, 1994; *Koops*, 1995; *Simpson and Schulenegger*, 2003). However, these usually fail to include detailed sedimentary information making difficult the establishment of a clear relationship between imposed tectonic, landscape and sedimentation (*Egholm et al.*, 2013). Although the geologic modelling scale is useful because it encompasses qualitative and quantitative investigations common to physical geography, process geomorphology, palaeoclimatology, stratigraphy and geodynamics (*Koltermann and Gorelick*, 1992; *Bishop*, 2007; *Jerolmack*, 2011), it presents major challenges related to the way physical processes are modelled and the assumptions that are made.

Willgoose (2005) published a comprehensive review of landscape evolution codes in the geomorphology community. The author noted that fluvial modules are the core of these codes and are all similar in principle, but vary in the constitutive equations used to model natural processes. Most of these codes use an explicit transport capacity model with mass balance for overland and river flow.

Alongside landscape evolution codes, stratigraphic codes are designed to track the nature and geometry of sedimentary infill. Three categories have been proposed to tackle the problem of sediments distribution: (1) geometric (*Harbaugh and Bonham-Carter*, 1970), (2) diffusive (*Granjeon and Joseph*, 1999), and (3) hydraulic (*Tetzlaff and Harbaugh*, 1989). This breakdown is effective at describing the core modules of each specific code, but stratigraphic codes often use a hybrid formalism of two or more of the above approaches with various level of complexity. Stratigraphic codes are generally multi-processes and combine simplified descriptions of natural processes in such a way that continuity of mass is conserved (*Paola*, 2000).

Until recently, geomorphic and stratigraphic codes were generally separated. Increasing demand for solving geomorphic changes and track sedimentary record simultaneously raised to the generation of new codes (*e.g.* CHILD: *Gasparini et al.* (2004), or ROMS: *Warner et al.* (2008)) and has motivated the development and implementation of the approach we present in this paper. Our model is based on a mixed Lagrangian and semi-empirical methodology to simulate open-channel flow, mass wasting processes and soil creep. Open-channel flow is simulated using a modified Lagrangian form of the shallow-water equations. This latter technique has the advantage of allowing the surface flow to follow accurately the topography and also offers an alternative to purely diffusive approach used in other stratigraphic models (*Granjeon and Joseph*, 1999; *Nikora et al.*, 2002; *Heimsath et al.*, 2005). Mass wasting processes are modelled using a semi-empirical approach based on susceptibility maps for activation and a slope diffusion algorithm for transport (*Rickenmann and Zimmermann*, 1993; *Horton et al.*, 2013).

First, this paper presents the combined open-channel flow and non-uniform sediment transport method, and the semi-empirical diffusive mass wasting method. Then, the parallel implementation and numerical approaches making the core of the numerical code, called LECODE, are briefly described. Finally, a set of generic experiments focusing on assessing the influence of contrasting erodibility (a coefficient controlling the rock capacity to be dismantled by channel flow) on landscape dynamics, sediment supply evolution and drainage network development in a

synthetic active bedrock landscape is presented in order to illustrate the potential of the method for landscape and sedimentary system evolution modelling.

2 Simulated processes & governing equations

2.1 Open-channel flow

LECODE uses a modified 2⁺ dimensional Lagrangian model which could be seen as an hybrid approach inspired by the simplified Marker-and-Cell theory (*Tetzlaff and Harbaugh*, 1989; *Griffiths et al.*, 2001; *Tetzlaff and Schafmeister*, 2007) and the Path-Sampling method (*Mitasova and Mitas*, 1993; *Mitas and Mitasova*, 1998; *Mitasova et al.*, 2004). Lagrangian momentum tracers, or *flow walkers*, that represent depth-averaged fluid properties (*e.g.* volume, sediment discharge, sediments proportion) are tracked through a triangulated irregular network (TIN) that characterises the field variables (*e.g.* depth and bed elevation). For each flow walker, the momentum equation is solved in its Lagrangian form to reduce numerical dispersion (*Thomas et al.*, 2006), whilst the continuity equation is solved using a semi-empirical technique based on stream classification approach (*Rosgen*, 2003). As flow walkers accelerate and decelerate due to interactions with topography, erosion and deposition are induced on a regular stratigraphic mesh. The model presented here simulates fluid flow and sediment transport in the horizontal plane and depth and deposition in the vertical plane. Non-uniform total-load sediment transport is simulated by using a non-equilibrium approach, dividing the sediment mixture into size fractions and accounting for the effects of hiding and exposure (*Wu*, 2007). Historical erosion and deposition are represented by a mixing layer approach (*Hirano*, 1972).

2.1.1 Open-channel flow equations

It is possible to obtain two key equation sets for a single flow walker from Newton's laws of motion: (*i*) the law of conservation of mass for an incompressible fluid and (*ii*) the Navier-Stokes momentum equations for an incompressible fluid (*Lane and Richards*, 1998). In two dimensions, assuming that the fluid is homogeneous, incompressible and at constant temperature, and using a steady water flow that is close to kinematic wave approximation (*Mitasova et al.*, 2004), the continuity or mass conservation equation can be expressed as:

$$\frac{\partial A}{\partial t} = -\nabla \cdot (A\mathbf{v}) = 0 \quad (1)$$

where A is the flow area and \mathbf{v} is the horizontal flow velocity vector. Using empirical law we define a width (w) to depth (h) ratio ($\alpha(S)$) based on topographic slope S such as $A = \alpha(S)h^2$. A stream classification system (*Rosgen*, 2001, 2003) is used to compute $\alpha(S)$ based on a quantitative description of a combination of river features (*Juracek and Fitzpatrick*, 2003; *Hey*, 2004; *Wohl et al.*, 2005).

In Cartesian coordinates, the simplified depth-averaged shallow water momentum equations can be written as:

$$\frac{D\mathbf{v}}{Dt} = -gR\nabla H + \frac{c_2}{\rho}\nabla^2\mathbf{v} - c_1\frac{\mathbf{v}|\mathbf{v}|}{h} \quad (2)$$

where $\frac{D\mathbf{v}}{Dt}$ is the Lagrangian derivative of horizontal flow-velocity vector with respect to time, H the water surface elevation, ρ the fluid density, c_1 is the bottom friction coefficient, c_2 the coefficient of lateral friction and gR represents the specific gravity of the flow. The flow acceleration is governed by (*i*) gravity and the elevation of the water surface, (*ii*) lateral friction experienced by the fluid and (*iii*) bottom friction.

In arriving at equations 1 and 2, a number of simplifying assumptions have been made. Because of the relative small dimension of the channels, the Coriolis force, horizontal variations in atmospheric pressure and water surface wind stress terms have been neglected (*Lane and Richards*, 1998). It has been assumed that the hydrostatic pressure distribution (*Vreugdenhill*, 1994) and constant density hold over the flow depth. In addition the shear stress and dispersion terms have been modelled very simply, assuming that dispersion dominates turbulent momentum diffusion, and terms involving cross-derivatives have been neglected (*Westerink*, 2003).

2.1.2 Friction coefficients

Bottom friction coefficient c_1 is approximated using the approach of Manning combined with a Chezy's type form for equation 2 (assuming that the diffusion term is very small and that the flow is steady) (*Tetzlaff and Harbaugh*, 1989; *Griffiths et al.*, 2001). Thus:

$$c_1 = gR \frac{n^2}{h^{1/3}} \quad (3)$$

where n is the Manning roughness coefficient. The values of n are determined empirically and are available for open channel flow (*Arcement and Schneider*, 1984; *McCuen*, 1998).

Lateral shear stress plays an important role when looking at sediment distribution in natural rivers (*Yang et al.*, 2004; *Wu*, 2007). As this approach is based on a depth averaged formalism to represent the flow, helical flow that takes place in river meander is not represented. However, erosion and deposition at river bends are also affected by higher shear stresses associated with higher velocities on the outsides and by lower velocities and shear stress on the inside of bends (*Crosato*, 2008). By keeping the lateral friction in the governing equation, this phenomena is mimicked even though rates of erosion and deposition are underestimated compared to natural streams.

2.1.3 Sediment erosion, transport & deposition

Three main modes of sediment transport are distinguished: wash load, suspended load and bed load. The model we present here is concerned with the latter two modes. The suspended load fraction is made up of particles that are held in suspension by turbulent eddies, whilst the bed load fraction is made up of particles that roll, slide, or saltate along the bed. In LECODE, the water column is treated as a single bed-material load layer, since computational efficiency is of key importance and because this technique is less reliant upon empiricism (*Langendoen*, 2000).

Settling velocity of sediment particles The settling velocity equation proposed by *Zhang* (1989) applies to the entire range of viscous to turbulent conditions and is implemented in LECODE:

$$w_s = \sqrt{\left(13.95 \frac{\nu}{d}\right)^2 + 1.09 \left(\frac{\rho_s}{\rho} - 1\right) gd} - 13.95 \frac{\nu}{d} \quad (4)$$

Here w_s denotes the sediment's fall velocity, d the diameter of the sediment particle, ρ_s and ρ density of sediment and density of water and sediment mixture respectively, g the acceleration due to gravity, ν the kinematic viscosity of the fluid.

Non-equilibrium transport model For the determination of sediment transport in a non-uniform sediment mixture, it is convenient to divide the mixture into several size classes (*Zhang*,

1989; *Wu et al.*, 2000). For each size class k , a simplified sediment transport can be derived from *Wu* (2007) in a Lagrangian context:

$$\frac{Dc_k}{Dt} = -\frac{\beta_t w_{sk}}{h} (c_k - c_k^*) \quad (5)$$

Equation 5 assumes that mixing coefficients of the suspended sediment are small and c_k is the depth-averaged concentration of sediment k , c_k^* is the equilibrium sediment concentration, β_t is the adaptation coefficient and can be estimated using the formula proposed by *Wu* (2007).

The net flux of sediment at the bed equals the change in bed elevation due to erosion and deposition of each size fraction. The bed elevation change by size fraction can be formulated using the Exner equation (*Yalin*, 1972; *Paola and Voller*, 2005) as:

$$(1 - \lambda) \frac{\partial z_k}{\partial t} = \left(\frac{\varepsilon \beta_t w_{sk}}{h} (c_k - c_k^*) \right) \quad (6)$$

where λ is the bed porosity and z_k the bed deformation of the sediment class k . ε defines the erodibility term which is equal to 1 for non-cohesive materials and < 1 for cohesion materials when accounting for elevation change due to erosion.

Based on *Wu* (2007), the equilibrium sediment concentration c_k^* can be expressed as:

$$c_k^* = \frac{q_{sk}^* + q_{bk}^*}{Uh} \quad (7)$$

with q_{sk}^* the equilibrium transport rate of the class k of suspended load per unit width:

$$q_{sk}^* = p_{bk} \sqrt{\left[\frac{\rho_s}{\rho} - 1 \right] g d_k^3} \left[2.62 \cdot 10^{-5} \left(\left[\frac{\tau}{\tau_{ck}} - 1 \right] \frac{V}{w_{sk}} \right)^{1.74} \right] \quad (8)$$

and q_{bk}^* the equilibrium transport rate of the class k of bed load per unit width,

$$q_{bk}^* = p_{bk} \sqrt{\left[\frac{\rho_s}{\rho} - 1 \right] g d_k^3} \left[5.3 \cdot 10^{-3} \left(\left[\frac{n'}{n} \right]^{1.5} \frac{\tau}{\tau_{ck}} - 1 \right)^{2.2} \right] \quad (9)$$

p_{bk} is the bed material gradation, V the depth-averaged velocity, n' is the Manning's coefficient corresponding to the grain roughness ($n' = 0.05 \cdot d_{50}^{1/6}$), τ is the shear stress and τ_{ck} is the critical shear stress which accounts for the hiding and exposure effects (*Yang and Wan*, 1991; *Wu*, 2007).

2.2 Mass wasting

Mass wasting encompasses different processes such as landslide, debris flow or slump. A considerable number of approaches have been developed to predict specific types of mass wasting, which can be generally divided into three groups: (*i*) empirical-statistical methods (*Hsu*, 1978; *Corominas*, 1996; *Rickenmann*, 1999), (*ii*) analytical methods (*Sassa*, 1988; *Hungr*, 1995; *Hurlimann et al.*, 2007) and (*iii*) numerical methods (*Denlinger and Iverson*, 2004; *Crosta et al.*, 2009; *Hungr and McDougall*, 2009). Unified numerical simulation are difficult because the dynamic behaviour of each process is governed by different flow and impact mechanics in interaction with terrain features (*Christen et al.*, 2012). Moreover, at a regional scale and over geological time scales, purely numerical methods are almost impossible to constrain due to the uncertainty in modelling parameters. *Iverson et al.* (1998) suggest the use of simplified spatially distributed

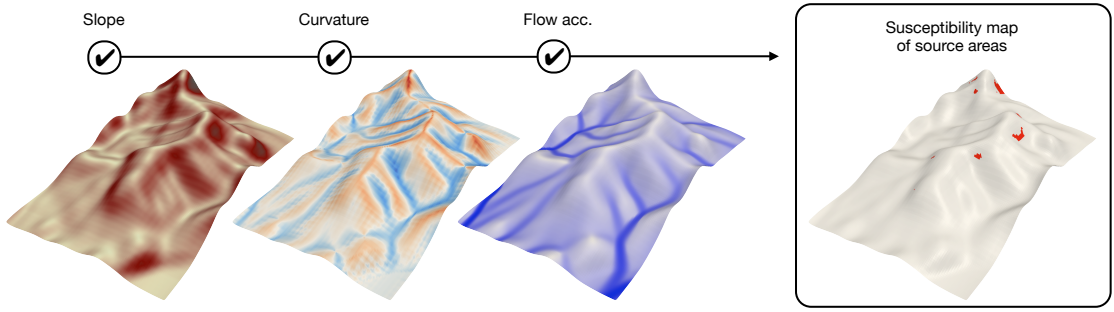


Figure 1: Illustration of the combination of various criteria for the assessment of mass wasting source areas. Slope, plan curvature and flow accumulation are computed in LECODE to assess regions prone to mass wasting (the red zones on the right surface). Sediments are available through all the model in this example.

models for regional case studies based on empirical or semi-empirical approaches (*Johnson and Rodine, 1984; Rickenmann, 1999*). LECODE considers a simplified approach that is not highly parameter dependant and that can provide first order mass wasting impacts at regional scale with minimum data requirements. The method consists in (*i*) assessing the region prone to mass wasting (conditional threshold), (*ii*) estimating the volume of sediment based on mass wasting susceptibility map, and (*iii*) propagating the sediment on the downslope areas using a diffusive approach.

2.2.1 Susceptibility maps

A combination of four relevant criteria must be satisfied for the initiation of a mass wasting processes: (*i*) terrain slope gradient must be higher than the defined limit, (*ii*) plan curvature, which can be used to delineate source area geometry must be larger than the defined threshold, (*iii*) flow accumulation, used as proxy for the mass-wasting event contributing area and water input, must be above the defined threshold, (*iv*) and sediment must be available (*Rickenmann and Zimmermann, 1993; Takahashi, 1981*). The source area delineation are handled with user-defined parameters. For all grid cells, each criterion is computed and datasets are then combined according to the following rule: a cell is a source area if all criteria are favourable for mass wasting initiation (Figure 1).

Flow accumulation Water input can be represented by the upslope contributing area (flow accumulation) as frequently done in distributed hydrological models (*Tarboton, 1997; Erskine et al., 2006*). The calculation of flow accumulation from a digital elevation model (DEM) is normally performed using the flow-direction algorithm, which determines how to drain the flow from each given cell in the DEM into the neighbouring cell(s) and then recursively calculates the flow accumulation for every cell (*Freeman, 1991*). Assuming that the flow from a cell can drain into one or more downslope neighbouring cells a multiple-flow-direction technique is implemented here based on the *MFD-md* algorithm proposed by *Qin et al. (2007)*.

Empirical law When the four conditions are met for activation, mass wasting can occur. The area of the source is estimated using a stream power model, linking the slope to the upslope contributing area (U_{ca}):

$$S_{th} = k_s U_{ca}^{-\theta_r} \quad (10)$$

where S_{th} is the slope threshold for initialisation, k_s the steepness index and θ_r the concavity index. An extensive list of parameters reflecting particular geologic regions or environments can be found in the literature (Rickenmann and Zimmermann, 1993; Heinemann, 1998; Horton *et al.*, 2008; Fischer *et al.*, 2012; Horton *et al.*, 2013). In LECODE implementation, the user has the possibility to define up to two separate curves identifying the lower limit (based on U_{ca}) for a debris flow source initiation (Horton *et al.*, 2013).

2.2.2 Downslope propagation

Once the assessment of the mass wasting source areas has occurred, the volume of sediment transported is evaluated using the difference between the actual surface slope and S_{th} . A propagation routine based on a diffusion algorithm is then used to transfer the sediment downslope. The diffusion approach consists in (*i*) a multiple-flow-direction algorithm (*FD8*) that controls the path and the spreading of the process (Quinn *et al.*, 1991) and (*ii*) the characteristic angle of static friction (θ) of each sedimentary class composing the triggered process controlling the runout distance.

2.3 Sediment diffusion

In LECODE, sediment diffusion assumes that a sediment moves downslope until it reaches its angle of static friction (θ), at a rate proportional to the tangent of the slope angle. Such an assumption is simplistic because natural agents such as air and water, phenomena such as mass wasting, and biological agents actually move sediment at rates that are not determined solely by slope (Heimsath *et al.*, 2005; Paola *et al.*, 2009). However, diffusion is a critical process that is required in long-term sedimentary process modelling (Granjeon and Joseph, 1999; Tetzlaff and Schafmeister, 2007) and thus has been implemented here.

Diffusion alone cannot explain the details of geological features such as rivers, valleys, channels, fans, nor the shapes of most erosional or depositional features that range in size from metre to kilometre scale, but diffusion can be seen as playing a significant role in all of these. In LECODE, the slope diffusion algorithm is used in conjunction with previously described sediment transport processes. In this context, diffusion represents secondary transport mechanisms such as soil creep and minor slumps that occur at a scale smaller than the size of one cell (typical cell size in LECODE varies from 25 m to 500 m).

A set of maximum stable slopes for each grain type is user specified. Each grain type requires the definition of two maximum stability slopes for on-shore and off-shore deposition. When deposited sediments angle exceed θ , deposits are diffused through neighbouring cells until the equilibrium slope is reached. The approach uses (*i*) a *FD8* multiple-flow-direction algorithm (Quinn *et al.*, 1991) similar to the one implemented for mass wasting, and (*ii*) assumes the existence of an *active layer* (Hirano, 1972). In this active layer, each sediment type diffuses at its own rate based on its angle of static friction and the topographic slope.

3 Implementation design

Here, we briefly describe the technical aspects related to LECODE forward model implementation. LECODE stands for *Landscape Evolution, Climate, Ocean and Dynamic Earth* model.

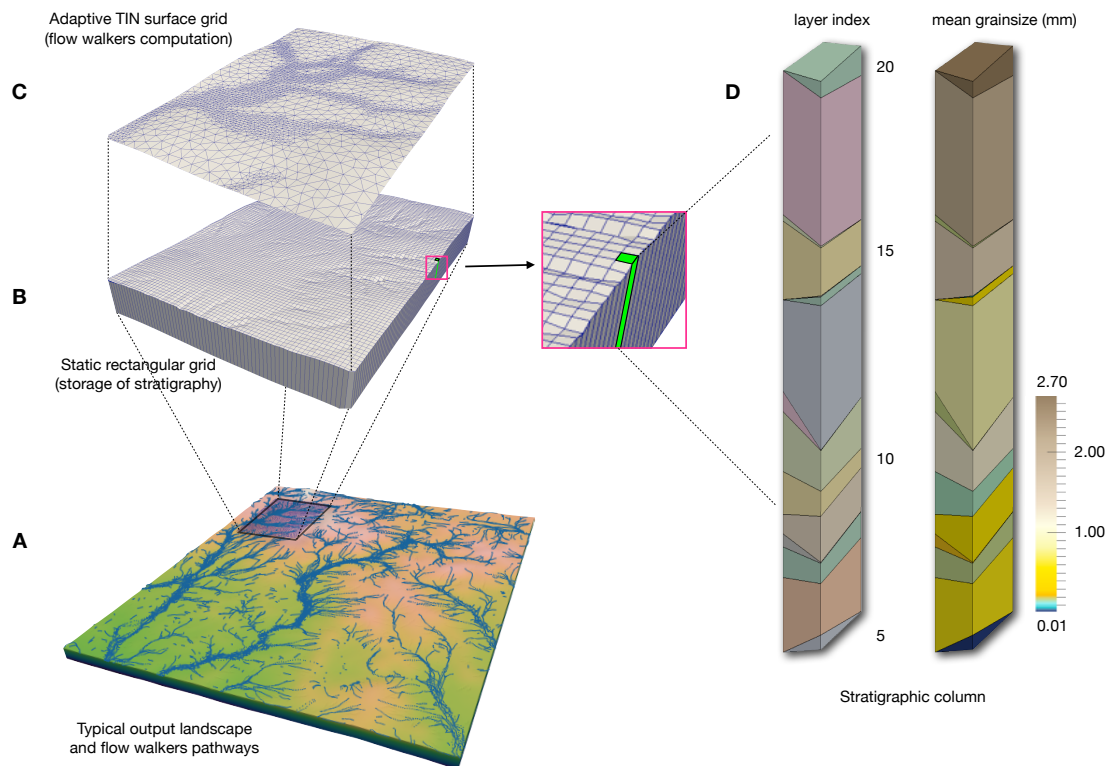


Figure 2: (A) Typical output of LECODE simulation. (B) Static rectangular grid used for storage of subsurface stratigraphy. (C) Computational adaptive TIN grid used to solve flow walker dynamics. (D) Stratigraphic columns are stored as a stack of layer indexes. Each layer contains information about layer age, grain size composition, relative sediment proportion as well as porosity.

3.1 Stratigraphy & flow computation

The simplicity of fixed regular grids have made them the framework of choice in nearly all numerical models (*Willgoose*, 2005). Nevertheless, the use of regular grid-based discretisation schemes have several disadvantages as noted by *Tucker et al.* (2001): (*i*) landform elements and stratigraphic bodies must be represented at a constant spatial resolution, (*ii*) under certain circumstances, the use of a regular grid introduces anisotropy; and (*iii*) use of a fixed grid makes difficult or impossible to model geologic processes that have a significant horizontal component such as fault displacement. Using a triangulated irregular network, or TIN, based mesh with movable nodes introduces a subsurface storage and information retrieval problem. To overcome these problems, *Clevis et al.* (2006) proposed an algorithm for mapping irregular data onto a static grid. LECODE adapts the idea proposed by *Clevis et al.* (2006) for meandering channels to long-term geomorphic and stratigraphic models. The spatial discretisation of the stratigraphic record and the method by which water and sediments are routed over the surface are done in two distinct referentials. Stratigraphic information is recorded in a fixed subsurface rectangular grid that underlies a self-adapting TIN over which flows are simulated (Figure 2).

3.1.1 Stratigraphic record

The stratigraphic evolution in LECODE is handled in a way common to several stratigraphic (*Tetzlaff and Harbaugh*, 1989; *Hutton and Syvitski*, 2008; *Dalman and Weltje*, 2012) and hydrodynamic (*Li and Amos*, 2001; *Warner et al.*, 2008) models. LECODE is capable of representing an unlimited number of user-defined non-cohesive sediment classes. Each class has fixed attributes of grain diameter, density, settling velocity and angle of friction. These properties are used to determine bulk properties of each bed layer.

The model has a regular orthogonal square grid in the horizontal plane. The initial sediment layers are represented by three-dimensional arrays with a user-specified, number of layers beneath each horizontal model cell. Each cell of each layer in the bed is initialised with a thickness, sediment-class distribution, porosity, and age. The mass of each sediment class in each cell can be determined from these values and the grain density. The age property tracks the time that deposition last occurred in that layer. The bed layers are modified at each time step to account for erosion, deposition and stratigraphy tracking. Thus, the grid evolves dynamically through time along the vertical axis and the grid-cell layers are treated as time lines. A new grid-cell layer is added at each user-defined time period.

3.1.2 Triangulated Irregular Network adaptive meshing

At specific time period which normally coincides with the creation of a new deposit layer, a new TIN grid is mapped over the stratigraphic grid. To ensure both code efficiency, as well as stability of flow walker solutions (equations 1 & 2), an innovative technique has been implemented. The approach consists in using flow accumulation values above a defined threshold to approximate areas where flow walkers will concentrate. For these areas a high resolution TIN mapping is required. In contrast, when flow accumulation values are relatively low, the probability of having flow walkers decreases and therefore a lower TIN resolution is generally sufficient. Figure 3 shows an illustration of the TIN adaptive remeshing capability based of flow accumulation and implemented in LECODE.

Depression-less algorithm During flow accumulation calculations over the stratigraphic grid, a preprocessing algorithm is used to fill the depressions and remove the flat areas before the flow algorithm is used (*Hengl and Reuter*, 2008). This depression-less algorithm is

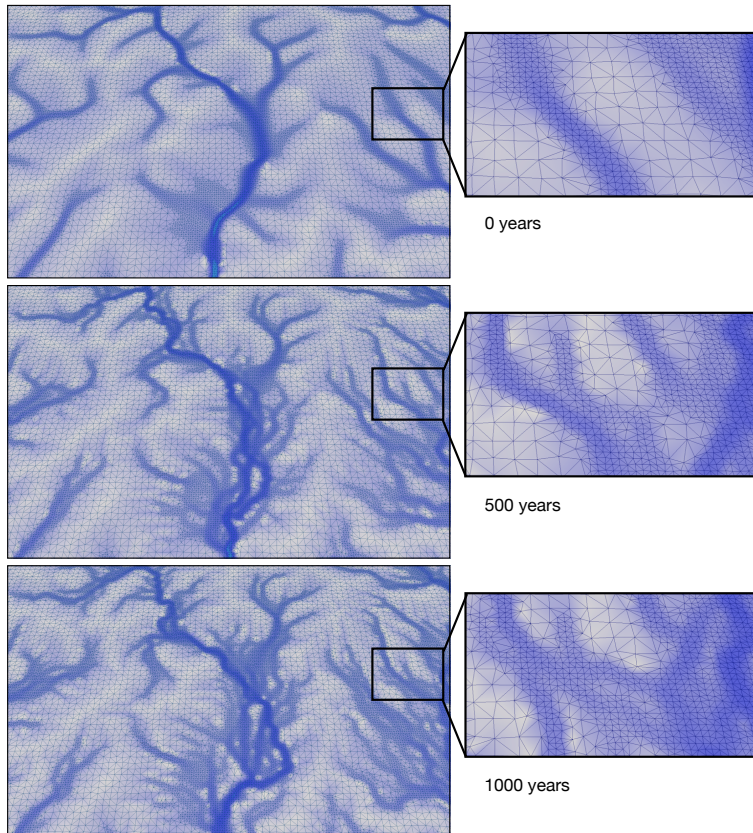


Figure 3: Flow accumulation snapshots illustrating development of a valley pattern through time due to cumulative effect of rain, rivers and mass wasting. The figure shows how the adaptive remeshing technique of the surface TIN is used in LECODE to compute flow walker dynamics. Panels on the right side present the evolution of the low and high resolution zones in a specific area of the valley.

required to properly determine the flow direction and to obtain hydrologically valid results for flow accumulation. Many preprocessing algorithms, often with an iterative process, have been proposed (*Jenson and Domingue*, 1988; *Planchon and Darboux*, 2001). Because of its simplicity and execution time, the algorithm developed by *Planchon and Darboux* (2001) is implemented in LECODE.

Flow accumulation and TIN mapping As described in section 2.2.1, the calculation of flow accumulation is performed using a multiple-flow-direction technique utilising the MFD-md algorithm proposed by *Qin et al.* (2007). With the flow accumulation values determined, a set of nodes within the stratigraphic grid are chosen at different spatial intervals corresponding to highest and lowest resolution areas. These points are then used to produce a constrained Delaunay triangulation grid based on the algorithm developed by *Shewchuk* (2001). Finally, the produced TIN grid elevations are interpolated using a bivariate interpolation and smooth surface fitting technique (*Akima*, 1978, 1984) to ensure a smooth and conform representation of the stratigraphic grid.

The procedure detailed above allows the adaptive remeshing of surface TIN grid during the simulation (fig. 3). Each of the new Delaunay grids ensures (*i*) the best resolution in places where flow accumulation values are high and (*ii*) smooth representation of stratigraphic grid elevation in places of lower resolution. This new method has the advantage of reducing the computational time of the overall simulation while preserving the stability and accuracy of flow walker hydrodynamic solutions.

3.2 Code parallelism

To increase LECODE's computational efficiency, a two-level mapping parallelism technique is employed. This method allows us to partly overcome the problem of sparse flow walkers. The first level of parallelism handles the mesh partitioning. Features and functions directly related to the mesh and its geometry such as stratigraphy evolution, TIN remeshing, mass wasting processes and slope diffusion are resolved and stored on each partition. The second level of parallelism is specifically designed to efficiently compute flow walker dynamics and handles changes in flow velocities, positions and sediment concentration.

3.2.1 Mesh partitioning

At the beginning of a simulation, stratigraphic nodes positions representing initial sedimentary layers are known. Once the regular surface has been generated, the set of nodes is partitioned into subdomains. Each subdomain can then be mapped onto a processor of a parallel architecture. For our purposes, we consider a mesh partitioner desirable if it produces subdomains of nearly equal size (where size is measured by number of nodes) and with as few nodes shared between processors (ghost nodes) as is reasonably possible. LECODE partitioner uses the Hilbert Space-Filling Curve method algorithm, a description of the method is found in *Zoltan* library (*Catalyurek et al.*, 2007; *Devine et al.*, 2009).

3.2.2 Flow walker parallelism

Flow walker parallelism is based on the load-balancing of the number of walkers amongst the processors available. Every time new walkers enter the system as stream flow or rainfall the total number of walkers is calculated and partitioned on the processors. This ensure that each processor has approximately the same number of flow walkers to compute. However, after several

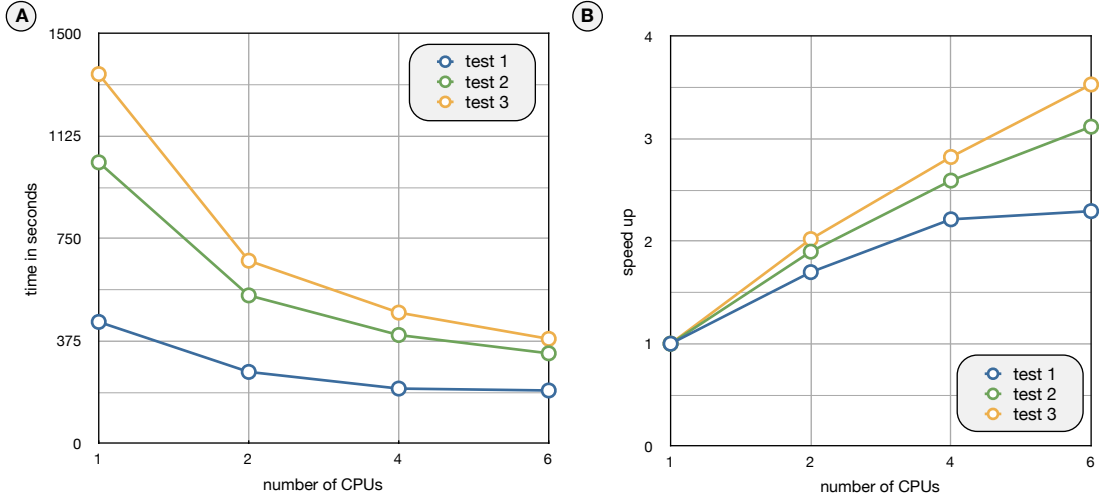


Figure 4: Performance tests for a series of 3 simulations. Graphics show (A) time versus CPUS and (B) speedup versus CPUS for each of the tests.

flow computation iterations walkers may die or exit the simulation space, thus leading to an unbalanced situation until the next walkers partitioning is performed, thus limiting the achievable performance speed-up.

3.2.3 Performance

To test the performance of the parallelisation, a set of simple experiments is produced. Test 1 was ran on a 300 per 400 mesh with a release of 20 flow walkers. Test 2 & 3 are ran on a 400 per 500 mesh but the total number of flow walkers released during the simulation varies from 200 for test 2 to 1000 for test 3. Each test finishes after the first output is produced. Thus, the simulation time corresponds to (*i*) the initialisation phase, (*ii*) the computation of a single distribution of flow walkers, (*iii*) the computation of the diffusion processes (creep as well as mass wasting), (*iv*) the construction of the output and (*v*) the finalisation phase. The set of tests has been performed on a computer with 2.7 Ghz Intel Core i7 for a series of 1, 2, 4 and 6 processors each time. Results of the performance are presented in Figure 4. For comparisons, we use both the time (Figure 4(A)) and the speedup (Figure 4(B)). The latter refers to how much the parallel algorithm is faster than the corresponding sequential one. Three main observations can be made from these tests. First, parallel performance tends to be better for simulations with the largest mesh size and number of flow walkers (tests 2 & 3). Secondly, mesh partitioning produces better performance than the flow walker parallelisation technique; however, the flow walkers parallelisation scalability is quite efficient over the range of tested processors. Finally, based on the speedup graph (Figure 4(B)) it seems that the parallel performance decreases with an increase of processors number.

Overall, the parallel implementation performs well for large simulations involving hundreds to thousands flow walkers. To ensure best performance on larger architectures, like supercomputers, further work needs to be done to assess the scalability of the code parallelism and the amount of communications load.

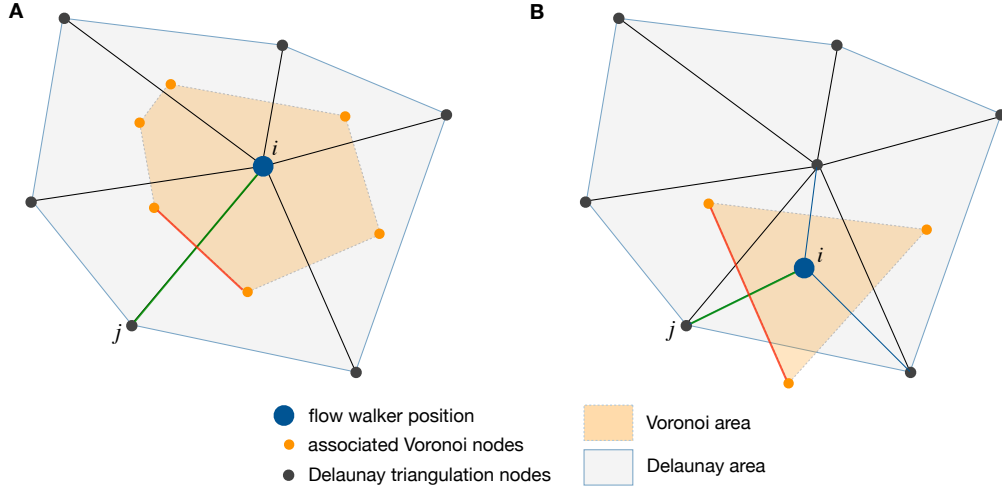


Figure 5: Finite difference approximation of the diffusion operator in the momentum equation. The flow walker position is defined at position i . (A) Flow walker i is positioned on a grid vertex, (B) flow walker i is inside the Delaunay cell.

4 Numerical methods

In LECODE, a decoupled approach (*Tannehill et al.*, 1997) is utilised to solve the governing equations at each time step. Two different solution methods for the equations are required: (i) one for the Lagrangian momentum and continuity equations solved on the TIN and (ii) one to solve the sediment transport equation on the stratigraphic mesh and to couple the solutions. This coupling is essential in order to ensure conservation of both mass and momentum (*Tannehill et al.*, 1997).

4.1 Momentum conservation

The simplified momentum equation (2) in Lagrangian form is solved using an explicit finite difference approach based on the Cash Karp Runge Kutta method with automatic time stepping (*Cash and Karp*, 1990; *Press et al.*, 2007). The method uses six functions evaluation to calculate fourth- and fifth-order accurate solutions. The difference between these solutions is then taken to be the error of the fourth-order solution. This error estimate is convenient for adaptive step size integration algorithms (*Press et al.*, 2007). The technique has the advantage of being fast and accurate (*Press et al.*, 2007; *Thomas et al.*, 2006).

Prior to the resolution of the momentum equation the diffusion operator needs to be discretise. The discrete form for the diffusion operator ($\nabla^2 \mathbf{v}$ in equation 2) is obtained using a Voronoi cell finite difference method (*Sukumar*, 2003) (Figure 5). The central-difference (cell-based) approximation for the derivative of \mathbf{v} normal to the Voronoi edge is given by:

$$\nabla^2 \mathbf{v}_i = \frac{1}{va_i} \sum_{j=1}^p \frac{\mathbf{v}_j - \mathbf{v}_i}{l_{ij}} m_{ij} \quad (11)$$

where p is the number of natural neighbours for node i ($n = 6$, $n = 3$ in Figure 5 A & B respectively). va_i is the area of the associated Voronoi cell (coloured in orange), l_{ij} is the distance between nodes i and j (green segment), and m_{ij} is the length of the Voronoi edge

associated with nodes i and j (red segment). On a regular grid, the difference scheme reduces to the classical finite difference method (*Sukumar*, 2003).

4.2 Mass conservation

Once the positions and velocities of all flow walkers have been updated an upstream finite difference schema coupled to an empirical approach is used to compute the new flow depth. First, the new flow area A in equation 1 is obtained such as:

$$A(s + \Delta s) = \frac{A(s)\mathbf{v}(s)}{\mathbf{v}(s + \Delta s)} \quad (12)$$

where s and $s + \Delta s$ are the previous and new position of the flow walker respectively. Then for each walker, a forward looking algorithm (global eight-neighbour algorithm or *GD8*, *Paik* (2008)) seeks the most sensible short term path to take and compute the adjusted slope for each flow walker. The method is based on a global grid search algorithm for non-dispersive flow path extraction and allows for more variability in flow directions in comparison to widely used non-dispersive algorithms (*Paik*, 2008). It has the significant advantage of reducing the uncertainty in the computation of flow paths.

Once the global slope for each walker has been updated the empirical stream classification provides the width to depth ratio $\alpha(S)$ which is then used to compute the new flow depth h .

4.3 Sediment transport

Since flow walkers are positioned on the automatically generated TIN and sedimentary evolution is computed on the regular stratigraphic mesh, exchange of information is required to determine values of flow parameters in the mesh. The region of influence of flow walker's is defined based for their computed width and depth. Cross-sectional shape of the flow walkers is assumed to be rectangular thus each underlying nodes of the stratigraphic mesh contained in the region of influence experiences a similar flow dynamic. To compute bed elevation (equation 6), the flow depth h , averaged velocity V , and concentration c are required at each of the considered nodes. Values for equilibrium transport rate of suspended q_s^* and bed q_b^* load are then fully determined based on *Wu* (2007) equations. The solution for the Exner equation (6) is solved explicitly:

$$z_k(t + \Delta t) = z_k(t) + \left(\frac{\Delta t \varepsilon \beta_t w_{sk}}{h(1 - \lambda)} (c_k - c_k^*) \right) \quad (13)$$

Depending of the active layer's sedimentary composition, the flow concentration is updated for each sediment class c_k define for each nodes. The concentration values for each flow walker is then updated based on the number of nodes present in the region of influence.

The solution algorithm is summarised in figure 6.

5 Application: Influence of contrasting bedrock erodibility on landscape dynamics

5.1 Model presentation

We illustrate the potential of LECODE forward model in the context of tectonic geomorphology. Here, we investigate the impact of contrasting bedrock erodibility on drainage development and

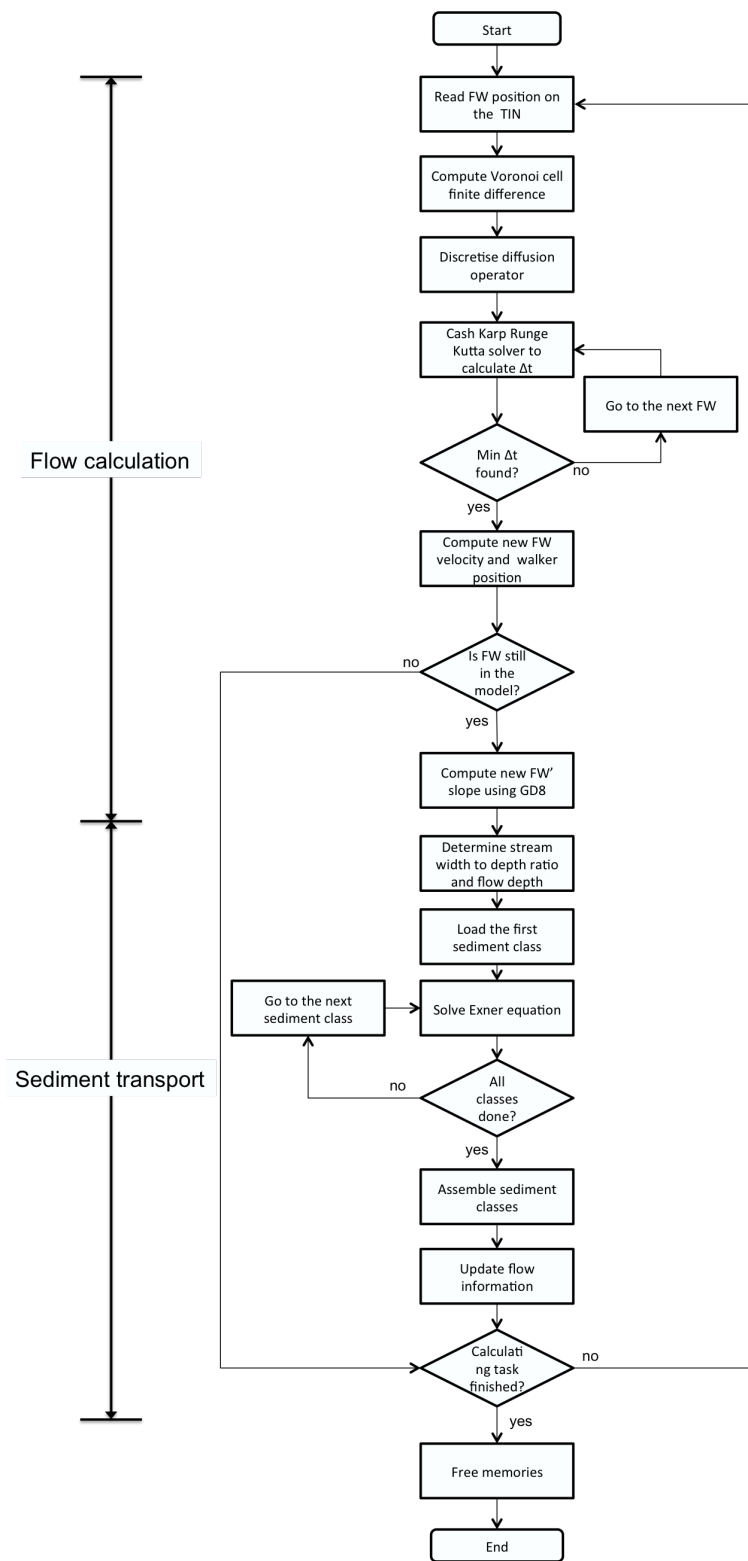


Figure 6: Flow chart summarising the sediment transport solution algorithm. FW: flow walker.

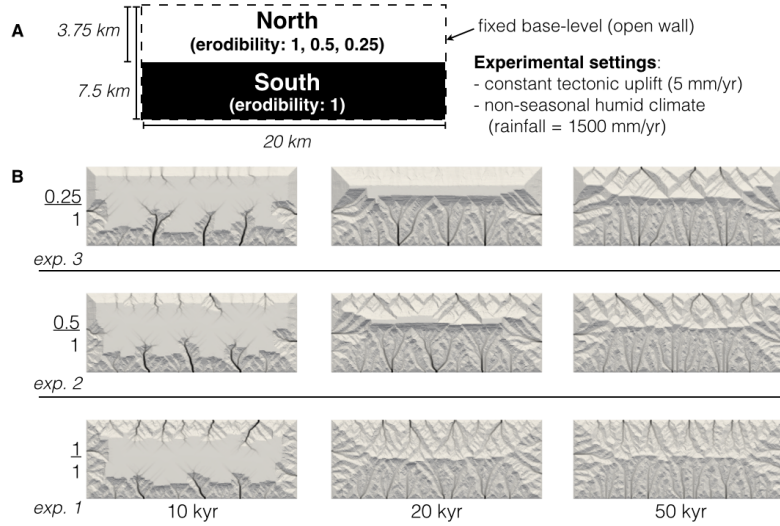


Figure 7: A. Experimental setup. B. Shaded map views of the TIN illustrating the evolution of the experiments surface topography at 10,000, 20,000, and 50,000 years. Darker colour indicates high flow accumulation values in channels. Experiment 1 (bottom) with homogeneous erodibility; experiment 2 (centre) with an erodibility of 0.5 to the north; and experiment 3 (top) with an erodibility of 0.25 to the north.

sediment yielding during the evolution of a plateau to a ridge in a bedrock landscape, under imposed climate and uplift. These two allogenic factors were set to represent a nonseasonal humid climate, with a mean annual rainfall of 1500 mm, and a constant tectonic uplift rate of 5 mm/yr with a fixed-elevation boundary condition (all material that reaches the edge of the model is removed in each surface flow step). This fixed elevation boundary condition imposes a constant base-level but precludes the formation of a piedmont at the base of the rising landscape. The initial setup for the three experiments, including the sole material properties, is summarised in Table 1. The three experiments extend over 20 km east-west and 7.5 km north-south, and only differ by a varying bedrock erodibility coefficient for the northern half of the model (Figure 7). The initial surface lays at the base-level (0 m) and its elevation varies randomly between -25 cm and + 25 cm over the all model.

Experiment 1 has a homogenous erodibility corresponding to a non cohesive basement material and represents our reference experiment. Experiments 2 and 3 are divided in a southern domain with non cohesive material (as in the experiment 1) and a northern domain with a basement material erodibility of 0.5 and 0.25, respectively. As basement material is detached from the original stratigraphic mesh, it becomes non-cohesive. These three experiments were performed on a mesh with a two-dimensional spatial domain discretised by 60,000 elements. Each model is run for 50,000 years, enough time for the topography to reach a steady-state. New sedimentary layers are recorded every 250 years, and results are output every 500 years.

5.2 Results processing

In order to examine and compare the experiments surface evolution we measured a series of quantitative metrics such as swath profiles, drainage slope-area distributions, sediment yielding budgets, and looked at alluvial terrace preservation.

North-south swath profiles, perpendicular to the ridge extension, were calculated for every timestep of each experiment across a centred 8.4 km wide east-west region. We limited the

Table 1: Experiments input parameters.

Property	Symbol	Unit	Value
MATERIAL PROPERTIES			
Density	ρ_s	$kg.m^{-3}$	2650
Grainsize	d	mm	0.2
Angle of friction	θ	—	0.011
erodibility (south)	ε	—	1
erodibility (north) – exp. 1	ε	—	1
erodibility (north) – exp. 2	ε	—	0.5
erodibility (north) – exp. 3	ε	—	0.25
FLOW PROPERTIES			
Water density	ρ	$kg.m^{-3}$	1010
Rainfall walker initial elevation	h	m	1.5
Manning coefficient	n	—	0.02
Flow walkers released per step		—	500
<i>Stream classes definition:</i>			
– Channel bed slope	S	—	0.0, 0.02, 0.2
– Width to depth ratio	$\alpha(S)$	—	200, 50, 20
MASS MOVEMENT PROPERTIES			
<i>Conditional activation parameters:</i>			
– Surface slope threshold	S_{th}	—	0.011
– Surface curvature threshold		—	0.1
– Flow accumulation threshold		—	1
Steepness Index	k_s	—	0.05
Concavity Index	θ_r	—	0.0

swath profiles to this central region to ensure the ridge is linear with all outlets located either north or south of the experiments. These profiles, including the mean, maximum and minimum elevations, are presented in Figure 8 alongside a corresponding shaded map view of the experiment's surface topography. They have been used to assess the headward migration of channels, the lifespan of the plateau during concurrent uplift and erosion processes, the position and elevation of the ridge divide through time, and examine the dominant process controlling the landscape morphology from the divide to the edge of the models.

Models' steepest slope and contributing area data, presented in Figure 9, have been calculated from the 50 m by 50 m gridded surface of the stratigraphic mesh using Grass GIS (*GRASS Development Team, 2012*) modules *r.param.scale* (*Wood, 1996*) and *r.watershed* (*Ehlschlager, 1989*), respectively. The resulting slope angles have been transformed to slope ratios, and the flow accumulation, computed using a single flow direction method, multiplied by the unit cell area to obtain a contributing drainage value for each cell of the model. These plots provide a robust metrics allowing for a direct comparison of the drainage distribution and evolution within and between LCODE models as suggested by various authors (*e.g., Willgoose, 1994; Tucker and Bras, 1998*). They will also facilitate future comparison with other landscape evolution models predictions.

Elevation data were used as well to compute the evolution of the average sediment yielding rate for the north and south flanks of the ridge (Figure 10), allowing us to explore the variation of sediment supply through time and link differential erodibility to contrasting but synchronous sedimentary record at regional scale.

Finally, alluvial sediments and a series of strath terraces were extracted from the model stratigraphic grid. Individual layers of alluvial deposits are recorded every 250 years. The evolving distribution of the alluvial deposits is presented in Figure 11. Alluvial terraces have been coloured based on their deposition age. They have been used to examine channel avulsion, aggradation and degradation processes in a steady-state landscape.

5.3 Results and discussion

5.3.1 Surface morphology and dynamics

Experiment 1 results allow to understand the degradation of a plateau and its dynamic evolution to a ridge with a constant base-level and imposed tectonic uplift and climatic forces. The minimum, mean, maximum topographic profiles extracted from the swath profiles on Figure 8 (bottom) provide information about the surface dynamics.

At 10,000 years, the minimum elevation profile allows to estimate the retreat rate of the plateau escarpment (*i.e.* a mean knickpoint migration rate) of approximately 23 cm/yr to the north and 25 cm/yr to the south. The small difference in migration rates between the two diverging drainages results from the limited dimension of the swath compared to the whole model (Figure 7B). The shaded map view highlights that while one major channel exists to the south of the plateau, three smaller channels are present to the north. These latter are degrading the plateau more homogeneously in space, limiting the influence of a unique channel. Additionally, the concavity of the minimum elevation profile, with a slope inflection around 2.1 km to the south, allows us to estimate the transition between hillslope dominated and channel dominated processes in the valleys.

The maximum elevation profile illustrates the survival of the plateau. Near the northern and southern edges of the experiment the maximum elevation profile becomes steeper and more linear suggesting that the threshold slope imposed for hillslope processes dominates. As the model edge elevation is constant its elevation represents the experiment base-level. Near the edge, the resulting tectonic uplift gradient has a strong control on the landscape response and

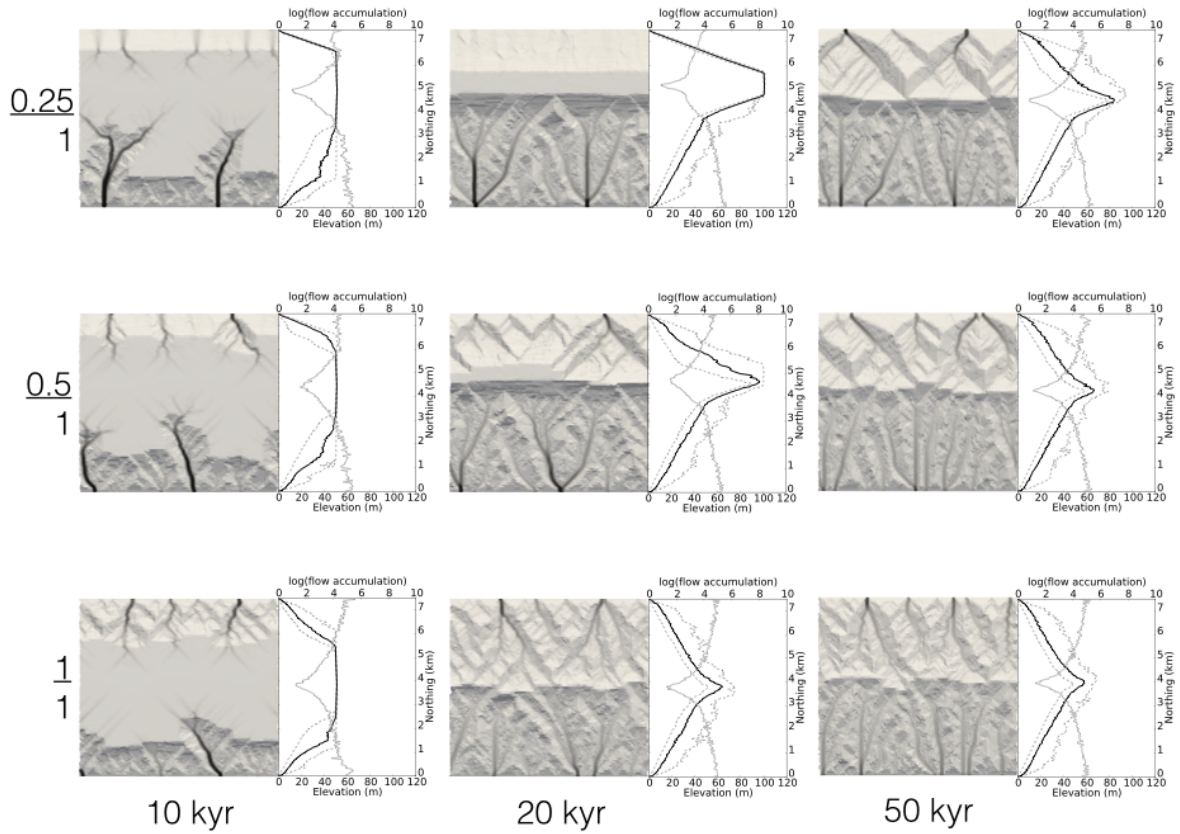


Figure 8: Compared evolution of the minimum, maximum (dashed lines) and mean (bold black line) elevation profiles calculated along a north-south swath corresponding to the shaded surface map (note the ten times vertical exaggeration) for experiments 1 (bottom), 2 (centre) and 3 (top). A logarithmic representation of the mean flow accumulation profile (grey line) highlights the position of the main drainage divide.

the first cells of the model are in an equivalent situation to the foot-wall of a normal fault with no sedimentation on the hanging-wall (*e.g.* *Petit et al.*, 2009). Thus, the maximum elevation profile also shows that on the dimension of tectonically-controlled faceted spurs in the context of varying erodibility. Cannot understand this sentence I think a verb is missing somewhere...

The mean elevation profile illustrates the general landscape trend. To the north of the plateau, this profile is very similar to the minimum elevation profile, suggesting that the whole landscape morphology is strongly influenced by the valleys. To the south, the mean elevation profile is closer to the maximum elevation profile, suggesting that hillslope processes are quite important. The noticeable contrast between the mean and minimum elevation profiles emphasises the importance of the unique channel described above, in controlling degradation.

The minimum of the mean flow accumulation curve indicates the northing position of the main drainage divide. In Experiment 1, the main drainage divide position is oscillating around the centre of the model, at an northing coordinate of 3.75 km.

At 20,000 years, the plateau has been entirely degraded, leaving a linear ridge with a main drainage divide and two separated drainage. The sawtooth shape of the maximum elevation profile indicates that the most elevated part of the relief are still subjected to readjustment. The minimum and mean elevation profiles show very similar patterns, and their concavity, with a slope inflection around 3.2 km, illustrate the transition between headwaters hillslope dominated and channel dominated processes in the valleys, and in the general landscape, respectively. The relief, corresponding to the difference between the maximum and minimum elevation profiles, is more marked upstream of the edge-controlled faceted scarps, and downstream the hillslope dominated ridge top, where channel incision controls the landscape.

At 50,000 years, the maximum elevation profile becomes smoother and the characteristics of the landscape described previously remain, suggesting the experiment reached topographic steady-state. The ridge mean elevation is steady at about 58 m above base-level.

We compare the results presented above with the two additional experiments' results in order to analyse the influence of contrasting erodibility on this system. Experiment 2 (0.5/1) and 3 (0.25/1) shaded surfaces, and minimum, mean, maximum profiles are presented in Figure 8 (centre) and (top), respectively.

At 10,000 years, the position of the main drainage divide, defined from the mean flow accumulation curve, is shifted toward the North inside the lower erodibility domain. In experiment 2, the knickpoint migration rates estimated from the minimum elevation profile are 16 cm/yr to the north and 31 cm/yr to the south. In experiment 3, these reach 14 cm/yr and 36 cm/yr to the north and south, respectively. The substantial difference between these values is a direct consequence of the contrasting erodibility. To the north, the lower erodibility is limiting bedrock detachment near headwaters. Whereas, to the south, the contributing drainage area of the channel is now more important increasing sediment transport capacity and promoting channel incision. The mean and maximum elevation profiles are very similar to each others and highly linear in both experiments, suggesting a very straight hillslope, controlled by a threshold slope processes.

At 20,000 years only a limited part of the plateau remains in experiment 2, while it is still largely preserved in experiment 3. The plateau elevation at this time reaches 100 m above base-level. As for experiment 1, the maximum elevation profiles near the southern edge suggest that the threshold slope imposed for hillslope processes dominates, thus controlling the shape of faceted spurs. However, to the north, this feature differs between experiments 2 and 3. In experiment 2 there is an evident asymmetry between north and south, with the northern faceted spurs extending further upstream and exhibit higher elevations on their top ridges. The relief is more important toward the north of the main divide. In experiment 3, the whole slope is straight

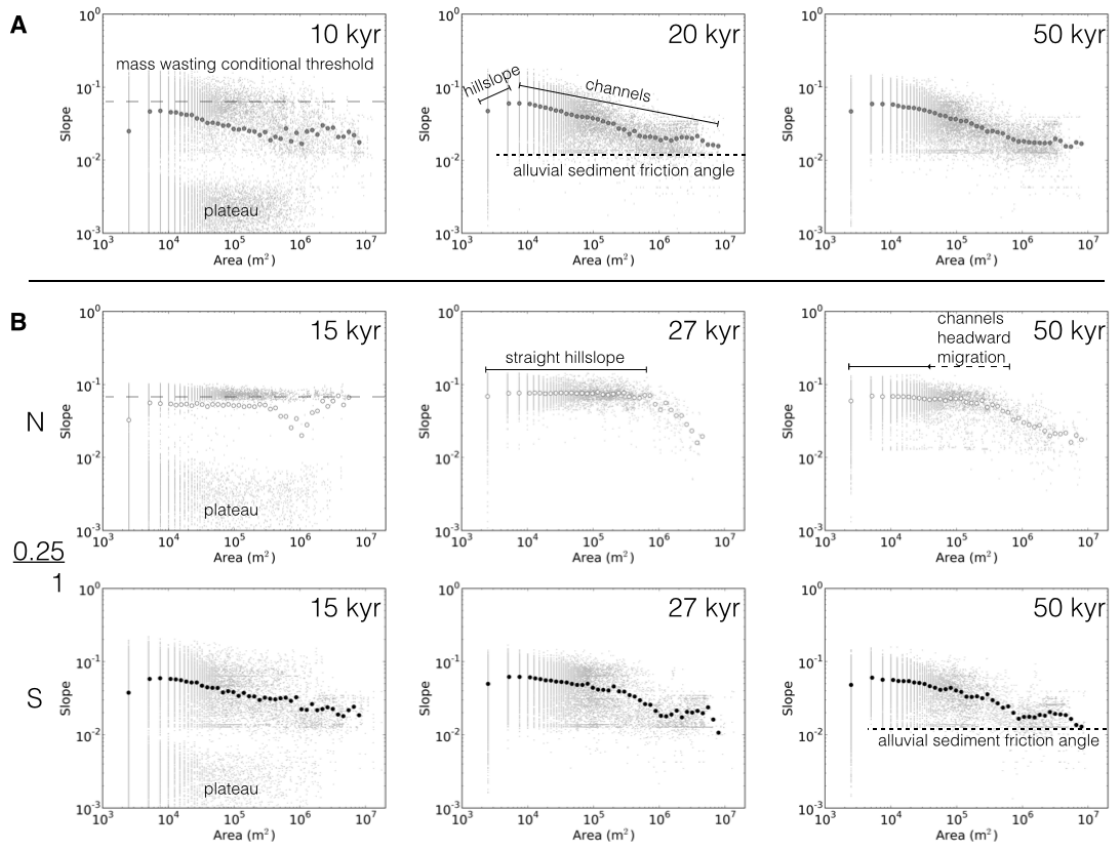


Figure 9: Evolution of the slope versus contributing area for the whole experiment 1 surface (A), and the separated north and south drainages of the experiment 3 (B).

with superimposed minimum, mean and maximum profiles indicating the absence of relief, and its angle is controlled by the imposed mass-wasting threshold.

At 50,000 years, the ridge mean elevation is steady at about 63 m and 81 m above base-level for experiment 2 and 3, respectively. Relief is more developed to the north of the main drainage divide, particularly in the case of experiment 3. Drainage has evolved as well and appears to be more distributed, particularly on the southern flank of the ridge. The faceted spurs are well developed on the northern edge of the model, in particular for experiment 3 where the overall landscape north of the main drainage divide is very dissected and intensely faceted suggesting a major control by channel incision in the valleys.

5.3.2 Evolution of the slope distributions

The relative influence of hillslope and channel processes is clearly evidenced in slope-area diagrams in Figure 9. The distribution of the slope-area data for the whole experiment 1 surface (Figure 9A) highlights the persistence of the plateau (low slope values over a large area observed at 10,000 years), an upper threshold controlled by conditional mass wasting, and a lower threshold controlled by the sediment angle of friction in aggrading channels. All data above the mass wasting conditional threshold can sustain a slope larger than the limit as these cells did not validate one or more of the four criteria necessary for initiating a landslide. The logarithmic-binned

averages exhibit a transition from a positive trend for low drainage areas to an negative trend for larger drainage areas. This change is well documented in modern landscapes (e.g. *Montgomery*, 2001) and corresponds to the transition from erosional hillslope processes to channel processes. Our experimental results suggest the presence of an attractor around 6500 m^2 . After 20,000 years the surface of experiment 1 appears to be largely controlled by channel processes.

The distribution of the slope-area data for the northern and southern drainage surface of experiment 3 (Figure 9B, top and bottom, respectively) indicates very contrasting evolutions. At 15,000 years, the data for the northern flank presents a marked dichotomy between the plateau and straight hillslopes. To the south, the distribution of the data is very similar to the one of experiment 1 with separate hillslope and channel domains that remains after the plateau is destroyed. At 27,000 years, the northern flank of the main drainage divide exhibits extensive straight hillslopes with an angle controlled by the mass wasting conditional threshold up to 10^6 m^2 where valley heads incise the straight surface and degradational channel processes start dominating. Between 30,000 years and 50,000 years, a clear headward migration of the channels occurred and consequently the negative relationship between slope and area in these degradational system is decreasing eventually leading to channel aggradation.

5.3.3 Balancing tectonic uplift

In our bedrock-landscape experiments sediment detachment is the key factor that controls erosion and inherently balances tectonic uplift. In order to evaluate the evolution of erosion through time and quantitatively compare the experiments we have calculated the mean sediment yielding rate for the north and south flanks of the main drainage divide in conjunction with the relative area of the experiment occupied by the south drainage (Figure 10).

Experiment 1 sediment yielding evolution (Figure 10 bottom), shows three distinct phases. For the first 18,000 years data illustrates an increasing sediment yielding phase that reaches a peak of sediment detachment rate of about $22 \text{ kt/km}^2/\text{yr}$ for both the north and south drainages. The timing of the peak appears to correlate with the maximum elevation of 90 m reached by the plateau before its destruction. This phase is followed with a rapid decrease (4,000 years) in sediment yielding rate (relaxation phase), then reaches a plateau and stabilises (steady-state phase). This stable erosion rate value of $14 \text{ kt/km}^2/\text{yr}$ balances the imposed tectonic uplift. Scattering of the data around the plateau value relates to small oscillations of the position of the divide, and deposition in the channels.

Experiment 2 (Figure 10) displays different trends for the north and south drainages. For the south drainage, the initial phase of increased erosion finishes by 18,000 years. The peak of sediment detachment rate is lower than for experiment 1 and reaches $18 \text{ kt/km}^2/\text{yr}$. The relaxation phase is relatively slow (7,000 years), then erosion stabilises to balance tectonic uplift. For the north drainage, the initial phase is less rapid (21,500 years) but yields to increased erosion rate ($25 \text{ kt/km}^2/\text{yr}$). The relaxation phase for the north drainage takes 8,500 years, after which the whole system appears to have reached a topographic steady-state where erosion balances tectonic uplift. The peak of sediment production coincides with both the maximum elevation of the plateau, and the initiation of the main drainage divide retreat toward the south. The divide retreat appears to stabilises as the system reaches steady-state around 30,000 years, by then the south drainage occupies about 56 % of the model surface.

Experiment 3 also displays different trends for the north and south drainages. For the south drainage, the initial phase of increased erosion finishes by 14,500 years but does not exhibit a peak of sediment detachment as for the other models, but instead directly stabilises to balance tectonic uplift. On the other hand the north drainage exhibits a slow initial build-up phase (30,000 years) that yields to a maximum erosion rate of about $23 \text{ kt/km}^2/\text{yr}$. The increased

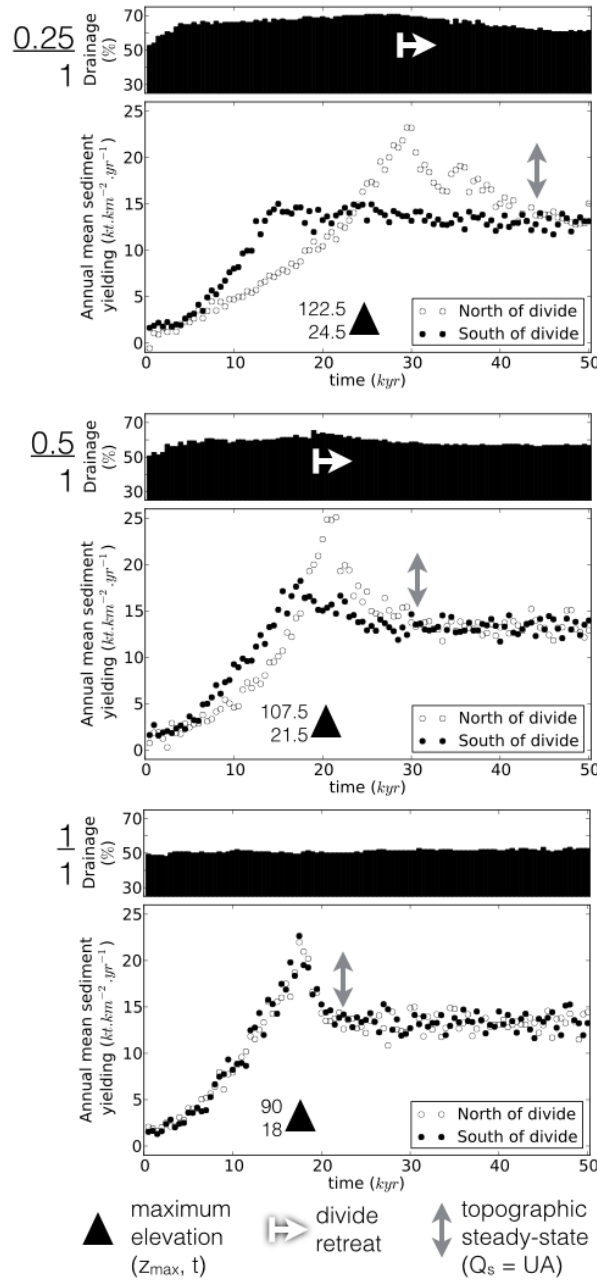


Figure 10: Evolution of the mean sediment yielding rate and the relative area occupied by the the south drainage for experiment 1 (bottom), 2 (centre), and 3 (top). See text for explanations.

yielding rate trend shows two parts with a slow linear increase for about 22,000 years, when the erosion rate value balances uplift rate, then it shows a steeper increase. This change relates to the onset of river incision. The relaxation phase takes about 13,000 years, after which the whole system has reached a topographic steady-state. In this case, the peak of sediment production apostates the maximum plateau elevation and coincides with the initiation of the main drainage divide retreat toward the south. The divide retreat appears to stabilise as the system reaches steady-state around 43,000 years, by then the south drainage occupies about 60 % of the model surface.

The absence of a peak in the long-term sediment yielding rate curve for the southern flank of the divide in experiment 3 contrasts with the two other experiments. This result confirms that rock hardness and other factors influencing erodibility play an important role in controlling evolution of topography, and the time for a dynamic system to reach topographic steady-state. Moreover, these results suggest that contrasting erodibility can stimulate an autogenic change in sediment supply through time. While we do not record sedimentation in the piedmont of the model, it is expected that there will be an important difference in the sedimentary record of the basins associated with the different sides of the main drainage divide.

5.3.4 Insights from the alluvial deposits

One of LECODE's strength lies in its capacity to record sedimentation history. Indeed, stratigraphic markers such as terraces and channel deposits, recorded by age intervals, provide valuable information to better understand the dynamics of the landscape at topographic steady-state (Figure 11). At steady-state, experiments 2 (Figure 11A) and 3 (Figure 11B top) with contrasting erodibility, present a richer alluvial record on the most erodible side of the divide (*i.e.* the south flank) and compared to experiment 1 (Figure 11B bottom). Alluviation occurs very early near outlets, on the floor of the stream dissecting the faceted spurs, and progress headward as landscape evolves. East-west cross-sections across three channels of experiment 2 (Figure 11A and C), allows to investigate the dynamics of the channels through the modelled stratigraphic record. Between 48,000 and 49,500 years, a stream flowing generally south has been subject to a series of east-west avulsions. Through time, epigenetic thalwegs formed by degradational channels are carved, and as the slope decreases these are filled with new sediments. Because of this frequent avulsion mechanism only part of the alluvial deposits are preserved. Strath terraces with flat surface expression perpendicular to the channel axis can be identified and their relative elevation can be used to unravel the cumulated uplift encountered by the local surface. The formation of strath terraces in LECODE is compatible with the sediment-loading model for strath formation proposed by *Hancock and Anderson* (2002). While the three experiments reached topographic steady-state as demonstrated from Figure 10, aggradational and strath terrace formation still occurs. Channel avulsion in our evolving ridge model appears to be an autogenic response of the system in which drainage evolves to minimise the distance between the sediment source and the outlet.

5.3.5 Discussion

LECODE implementation has been successfully applied to investigate landscape evolution under imposed tectonic and climatic factors. Experimental results satisfy established relationships for drainage network geometry and slope distribution, and provide quantitative information on the relative impact of hillslope and channel processes, sediment flux, and alluviation through space and time.

More specifically, the development and preservation of faceted landscapes as illustrated in Figure 8 is a very interesting result. Erodibility has a direct influence on the geometry of normal

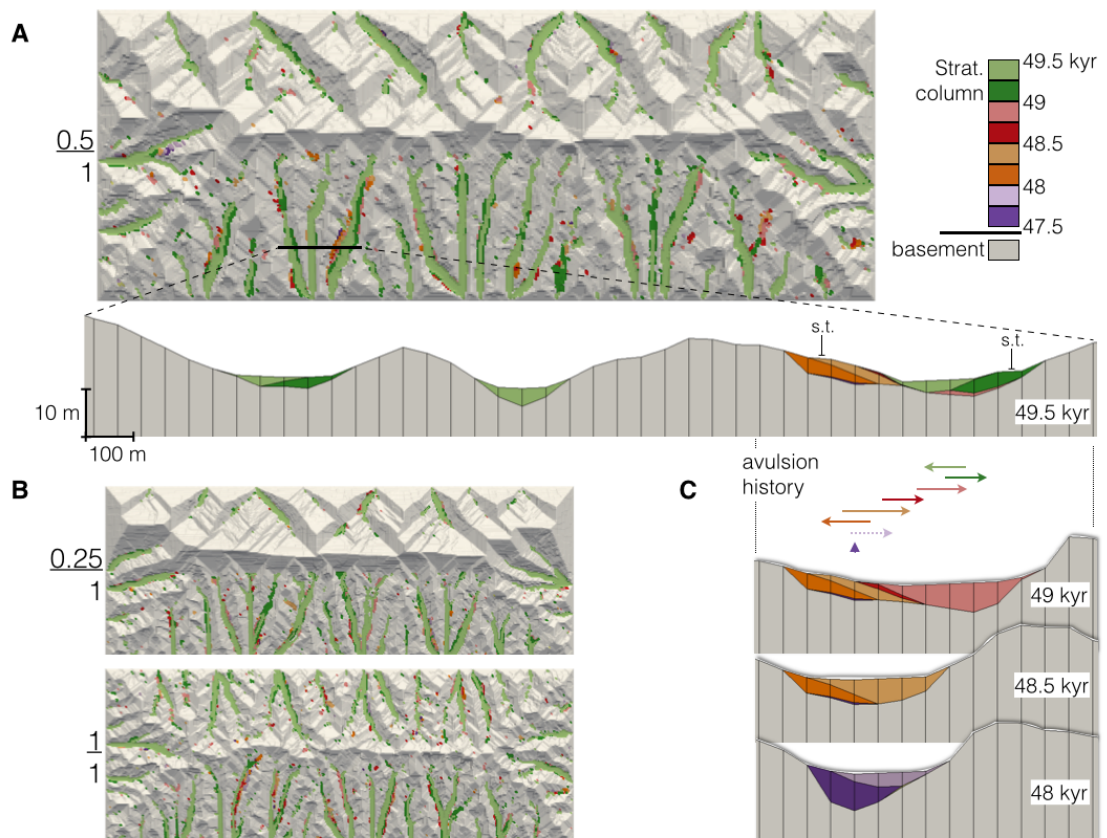


Figure 11: Representation of the distribution of alluvial deposits (coloured by age intervals) and exposed basement (grey). (A) Channels and terraces from experiment 2 provide rich information that can assist in understanding the evolution of the drainage through time (C). (B) Shaded relief representation of experiment 1 and 3 highlighting the surface distribution of channel deposits and exhumed basement. s.t.: strath terrace.

fault scarp on the edge of the experiments, and the preservation of marked landscape features such as outlets and deep incised valleys over time. This experimental result is in good agreement with recent observations from *Sharf et al.* (2013) suggesting that strong rocks in South Africa sustained steep slopes and high elevations while experiencing very limited tectonic activity throughout the Cenozoic. Experimental results from *Egholm et al.* (2013) suggested that the coupling between hillslope and channel erosion is critical for controlling the long-term preservation of mountain ranges. With LECODE we can quantify how channel and hillslope processes compete and evolve to control the landscape morphology.

For example, comparison of the retreat rates of the experimental plateaux (Figure 8) suggests that a contrasting erodibility promotes faster headward migration of the channels in the most erodible material. The contrast in bedrock erodibility, more than the actual erodibility, of an uplifting surface is critical for controlling the landscape morphology and the drainage network dynamics (Figure 9). The early persistence of straight hillslopes in the experiments 2 and 3 and the headward migration of channels is in good agreement with the concept of threshold hillslopes discussed by various authors (*Burbank et al.*, 1996; *Montgomery*, 2001; *Larsen and Montgomery*, 2012).

All experiments lead to a well-connected and coherent drainage network (Figures 7B, 8). After 50,000 years, the average spacing of the drainage outlets from the three experimental linear ridges range from 2.34 to 2.61 km, which is in good agreement with the 2.52 km predicted from the linear relationship proposed by *Hovius* (1996) (for a ridge half-width equal to 3.75km). As observed by various authors (*Simpson and Schlenegger*, 2003; *Castelltort and Simpson*, 2006), the drainage outlets configuration form early in the erosional history and subsequently remains relatively constant. While this is true for the outlets, our models suggest that the upstream drainage network configuration is more variable and that network reorganisation and drainage capture driven by channel avulsion occur through time, even after topography reached steady-state (Figures 10 and 11).

The evolution of mean sediment yield rates (Figure 10) provide a reliable estimate for the time it takes for a landscape to reach topographic steady-state. Calculated values are compatible with data collected in humid and tectonically active region such as New Zealand (*Hicks et al.*, 1996). In these models we identified three distinct phases in the evolution of erosion rate: (*i*) a growth phase, (*ii*) a relaxation phase, and (*iii*) a steady-state phase, each influenced by a dynamic response of hillslope and channel erosion processes to tectonic uplift. The absence of a peak in the long-term sediment yielding rate for the southern flank of the divide in experiment 3 contrasts with the two other experiments. As the south drainage area (A) grows rapidly, to occupy almost 68 % of the model by 12,000 years, the overall sediment transport capacity (Q_s) of the south of the drainage increases proportionally to balance the tectonic uplift rate (U), verifying the relationship for steady-state landscape ($Q_s = UA$) discussed by several authors (*e.g. Howard*, 1994; *Montgomery*, 2001).

This resulting increase in sediment transport capacity is sufficient to compensate tectonic uplift and the erosion rate stabilises to a steady-state value. This result confirms that rock hardness and other factors influencing erodibility play an important role in controlling evolution of topography, and influence the characteristic time required for a dynamic system to reach steady-state. In a bedrock landscape contrasting erodibility alone might be able to stimulate autogenic changes in sediment supply through time. While we do not record sedimentation in the piedmont for these experiments, it is expected that there will be an important difference in the sedimentary record in the basins associated with the different sides of the main drainage divide. Future work utilising the historic stratigraphic record stored in LECODE outputs (as in Figure 11) will provide new opportunities to study and link stratigraphic and geomorphologic records under imposed allochthonous factors.

6 Conclusions

We have presented a new methodology for modelling surface processes including hillslope and channel erosion and sedimentation. The equations for solving open-channel flow and non-uniform sediment transport in a semi-Lagrangian framework were successfully combined with semi-empirical diffusive mass wasting in a 2⁺-D-parallel model: LECODE. The implementation of the model is robust and computationally effective. Stratigraphic information is stored in a fixed subsurface rectangular grid and allows for the recording of historical erosion and deposition. This grid is overlaid by a self-adapting triangulated irregular network (TIN) used for surface flow calculations. A new adaptive remeshing technique of the TIN, based on depression-less and flow accumulation algorithms, ensures the dynamics of Lagrangian flow walkers, recording the surface flow properties, is accurate.

This mixed hydrodynamic/geomorphic/stratigraphic forward approach was successfully employed to investigate the evolution of an uplifting plateau with controlled base-level elevation under non-seasonal humid climate. We tested the influence of contrasting erodibility on landscape and drainage morphology and sediment supply evolution. The modelled landscapes satisfy established relationships for drainage network geometry and slope distribution, and provide quantitative information on the relative impact of hillslope and channel processes, sediment flux, and alluviation through space and time. This experimental work suggests that contrasting lithologies, and other factors influencing surface erodibility, in an otherwise perennial system, promote autogenic mechanisms which impact erosion rates through time. Previous work demonstrated the importance of rock strength (*Sharf et al., 2013*), an inverse function of erodibility, and the interlinks between landslides and rivers erosion (*Egholm et al., 2013*) to preserve topography over geological times. Although additional processes may take place in natural systems, we propose that the general approach to surface processes modelling, combining open-channel flow and non-uniform sediment transport with semi-empirical diffusive mass wasting - as implemented in LECODE - offers new opportunities to quantify and investigate joint landscape and sedimentary systems response to allogegenic factors. This method is designed to complement existing detachment-limited and transport-capacity limited models. The possibility to define and track a large number of individual material types makes this tool highly suitable to model source to sink problems where material dispersion is a key question that need to be addressed, such as alluvial exploration or basin analysis.

Acknowledgement

We would like to thank Guy Simpson and an anonymous reviewer for their valuable comments on an earlier version of this work. We thank our colleagues T. Poulet and M. Gazley for providing feedbacks on the manuscript. This work has been co-funded by the CSIRO Energy and the Minerals Down Under National Research Flagships.

References

- Akima H. (1978). A Method of Bivariate Interpolation and Smooth Surface Fitting for Values Given at Irregularly Distributed Points. *ACM Transactions on Mathematical Software*, 4(2).
- Akima, H. (1984). On Estimating Partial Derivatives for Bivariate Interpolation of Scattered Data. *Rocky Mountain Journal of Mathematics*, 14(1).

- Arcement Jr. G. and V. Schneider (1984), Guide for Selecting Manning's Roughness Coefficient For Natural Channels and Flood Plains. *United States Geological Survey Water-supply*.
- Bishop, P. (2007). Long-term landscape evolution: linking tectonics and surface processes. *Earth Surface Processes and Landforms*, 32 (3), 329–365.
- Bonnet, S., and A. Crave (2003). Landscape response to climate change: Insights from experimental modelling and implications for tectonic versus climatic uplift of topography. *Geology*, 31 (2), 123–126.
- Braun, J., and P. , van der Beek (2004). Evolution of passive margin escarpments: what can we learn from low-temperature thermochronology? *Journal of Geophysical Research* 109, F04009. DOI: 10.1029/2004JF000147.
- Burbank, D., J., Leland, E., Fielding, R., Anderson, N., Brozovic, M., Reid, and C., Duncan (1996). Bedrock incision, rock uplift and threshold hillslopes in the northwestern Himalayas, *Nature*, 379, 505–510.
- Cash, J. R., and A. H., Karp (1990). A variable order runge-kutta method for initial value problems with rapidly varying right-hand sides. *ACM Transactions on Mathematical Software*, 16, 201–22.
- Castelltort, S., and G. Simpson (2006). River spacing and drainage network growth in widening mountain ranges. *Basin Research*, 18, 267–276.
- Catalyurek, U., E., Boman, K., Devine, D., Bozdag, R., Heaphy, and L., Riesen (2007), Hypergraph-based dynamic load balancing for adaptive scientific computations. *IEEE In: Proc. of 21st International Parallel and Distributed Processing Symposium (IPDPS'07)*.
- Christen, M., Y., Buhler, P., Bartelt, R. Leine, J., Glover, A., Schweizer, C., Graf, B.W., McArdell, W., Gerber, Y., Deubelbeiss, T., Feistl, and A., Volkwein (2012). Integral hazard management using a unified software environment: numerical simulation tool "RAMMS" for gravitational natural hazards. *in: Koboltschnig, G.; Hbl, J.; Braun, J. (eds.) 12th Congress interpraevent*, 77–86.
- Clevis, Q., G. E. Tucker, S. T. Lancaster, A. Desitter, N. Gasparini, and G. Lock (2006). A simple algorithm for the mapping of tin data onto a static grid: Applied to the stratigraphic simulation of river meander deposits. *Computers & Geosciences*, 32 (6), 749–766.
- Corominas, J. (1996). The angle of reach as a mobility index for small and large landslides. *Can. Geotech. J.*, 33, 260–271.
- Crosato, A. (2008). Analysis and Modelling of River Meandering. *IOS Press*, 251 pp.
- Crosta, G. B., S., Imposimato, and D., Roddeman (2009). Numerical modelling of entrainment-deposition in rock and debris-avalanches. *Eng. Geol.*, 109, 135–145.
- Dalman, R., and G. J., Weltje (2012). SimClast: An aggregated forward stratigraphic model of continental shelves. *Computers & Geosciences*, 38, 115–126.
- Davis, W. M. (1899). The geographical cycle. *The Geographical Journal*, 14(5), 481-504.
- Denlinger, R. P., and R.M., Iverson, (2004). Granular avalanches across irregular three-dimensional terrain: 1. theory and computation, *Journal of Geophysical Research*, 109, 14 pp.

- Devine, K., E., Boman, L., Riesen, U., Catalyurek, and C., Chevalier (2009). Getting started with zoltan: A short tutorial. In: *Proc. of 2009 Dagstuhl Seminar on Combinatorial Scientific Computing*.
- Dietrich, W. E., D. G., Bellugi, L. S., Sklar, J. D., Stock, A. M., Heimsath, and J. J., Roering (2003). Geomorphic transport laws for predicting landscape form and dynamics. In: *the American Geophysical Union (Ed.), Prediction in Geomorphology*, 135, 103–132.
- Egholm, D., M., Knudsen, and M., Sandiford (2013). Lifespan of mountain ranges scaled by feedbacks between land sliding and erosion by rivers, *Nature*, 498, 475–478.
- Ehlschlager, C. (1989). Using the AT Search Algorithm to develop hydrologic models from digital elevation data. *Proceedings of International Geographic Information Systems (IGIS) Symposium 89*, 275–281.
- England, P., and P., Molnar (1990). Surface uplift, uplift of rocks, and exhumation of rocks. *Geology*, 18, 1173–1177.
- Erskine, R., T., Green, J., Ramirez, and L., MacDonald (2006). Comparison of grid-based algorithms for computing upslope contributing area, *Water Resource Research*, 42, 1–9.
- Fischer, L., L. Rubensdotter, K., Sletten, K., Stalsberg, C., Melchiorre, P., Horton, and M., Jaboyedoff (2012). Debris flow modeling for susceptibility mapping at regional to national scale in Norway. *Proceedings of the 11th International and 2nd North American Symposium on Landslides*.
- Freeman, T.G. (1991). Calculating catchment area with divergent flow based on a regular grid *Computers and Geosciences*, 17 (3), 413–422
- Gasparini, N. M., G. E., Tucker, and R. L., Bras (2004), Network-scale dynamics of grain-size sorting: implications for downstream fining, stream-profile concavity, and drainage basin morphology. *Earth Surface Processes and Landforms*, 29 (4), 401–421.
- Gilbert, G. K. (1895). Sedimentary measurement of Cretaceous time. *The Journal of Geology*, 3(2), 121–127.
- Granjeon, D. and P. Joseph (1999), Concepts and applications of a 3D multiple lithology, diffusive model in stratigraphy modeling. In: *Numerical Experiments in Stratigraphy*, SEPM (Society for Sedimentary Geology), 62, 197–210.
- GRASS Development Team (2012), Geographic Resources Analysis Support System (GRASS GIS) Software. *Open Source Geospatial Foundation*, <http://grass.osgeo.org>.
- Griffiths, C. M., C. Dyt, E. Paraschivoiu, and K. Liu (2001), Sedsim in hydrocarbon exploration. *Geologic Modeling and Simulation*. Merriam, D., Davis, J. C. - Kluwer Academic, New-York.
- Hancock, G. S., and R. S., Anderson (2002). Numerical modeling of fluvial strath-terrace formation in response to oscillating climate. *Geological Society of America Bulletin*, 114(9), 1131–1142.
- Harbaugh, J., and G., Bonham-Carter (1970), Computer Simulation in Geology. *Wiley Interscience New York*.
- Hasbargen, L.E., and C., Paola (2000). Landscape instability in an experimental drainage basin. *Geology*, 28, 1067–1070.

- Heinimann, H. R. (1998). Methoden zur Analyse und Bewertung von Naturgefahren, Bundesamt für Umwelt, Wald und Landschaft (BUWAL), 85, 247 pp.
- Heimsath, A. M., D. J. Furbish, and W. E. Dietrich (2005), The illusion of diffusion; field evidence for depth-dependent sediment transport. *Geology*, 33 (12), 949–952.
- Hengl, T., and H.I., Reuter (2008). Developments in soil science. *n: Geomorphometry: Concepts, Software, Application, v. 33, Elsevier, Amsterdam, Netherlands*, 707 pp.
- Hey, R.D. (2004). Evaluation of Natural Stable Channel Design Procedures. *ASAE Conference on Self Sustaining Solutions for Streams, Wetlands and Watercourses*.
- Hicks, D. M., J., Hill, and U., Shankar (1996). Variation of suspended sediment yields around New Zealand: the relative importance of rainfall and geology. *in: Erosion and Sediment Yield: Global and Regional Perspectives. International Association of Hydrological Science Publication, 236*, 149–156.
- Hirano, M. (1972), Studies on variation and equilibrium state of a river bed composed of nonuniform material. *Transactions Jap. Soc. Civ. Eng.*, 4, 128–129.
- Horton, P., M., Jaboyedoff, and E., Bardou (2008). Debris flow susceptibility mapping at a regional scale. *in: Proceedings of the 4th Canadian Conference on Geohazards*, 339–406.
- Horton, P., M., Jaboyedoff, B., Rudaz, and M., Zimmermann (2013). Flow-R, a model for susceptibility mapping of debris flows and other gravitational hazards at a regional scale. *Natural Hazards Earth System Science*, 13, 869–885.
- Hovius, N. (1996). Regular spacing of drainage outlets from linear mountain belts. *Basin Research*, 8, 2944.
- Howard, A. D., W. E., Dietrich, and M. A, Seidl (1994). Modeling fluvial erosion on regional to continental scales. *Journal of Geophysical Research: Solid Earth (1978–2012)*, 99(B7), 13971–13986.
- Howard, A. D. (1994). A detachment-limited model of drainage basin evolution. *Water resources research*, 30(7), 2261–2285.
- Hsu, K. J. (1978). Albert Heim: observations on landslides and relevance to modern interpretations. *in: Rockslides and Avalanches, edited by: Voight, B., Elsevier, Amsterdam, Netherlands*, 71–93.
- Hungr, O. (1995). A model for the runout analysis of rapid flow slides, debris flows and avalanches. *Can. Geotech. J.*, 32, 610–623.
- Hungr, O., and S., McDougall (2009). Two numerical models for landslide dynamic analysis. *Computer & Geoscience*, 35, 978–992.
- Hurlimann, M., V., Medina, A., Bateman, R., Copons, and J. Altimir (2007). Comparison of different techniques to analyse the mobility of debris flows during hazard assessment-Case study in La Comella catchment, Andorra. *in: Debris-Flow Hazard Mitigation: Mechanics, Prediction and Assessment, edited by: Chen, C.-L. and Major, J. J., Millpress, Netherlands*, 411–422.
- Hutton, E., and J., Syvitski (2008). Sedflux 2.0: An advanced process-response model that generates three-dimensional stratigraphy. *Computers & Geosciences*, 34, 1319–1337.

- Iverson, R. M., S. P., Schilling, and J.W., Vallance (1998). Objective delineation of lahar-inundation hazard zones. *Geological Society of America Bulletin*, 110, 972–984.
- Jenson, S.K., and J.O., Domingue (1988). Extracting topographic structure from digital elevation data for geographical information system analysis. *Photogrammetric Engineering and Remote Sensing*, 54 (11), 1593–1600.
- Jerolmack, D. J. (2011). Causes and effects of noise in landscape dynamics. *Eos Trans, AGU* 92, 44.
- Johnson, A. M. and J.R., Rodine (1984). Debris Flow. in: *Slope Instability*, edited by: Brunsden, D. and Prior, D. B., John Wiley and Sons, New York, USA, 257–361.
- Juracek, K.E., and F.A., Fitzpatrick (2003). Limitations and Implications of Stream Classification. *Journal of the American Water Resources Association*, 39 (3), 659–670.
- Koltermann, C. E., and S. M., Gorelick (1992). Paleoclimatic signature in terrestrial flood deposits, *Science*, 256 (5065), 1775–1782.
- Kooi H., and C., Beaumont (1994). Escarpment evolution on high-elevation rifted margins: insights derived from a surface process model that combines diffusion, advection, and reaction. *Journal of Geophysical Research*, 99, 12191–12209.
- Kooi H., and C., Beaumont (1996). Large-scale geomorphology: classical concepts reconciled and integrated with contemporary ideas via a surface process model. *Journal of Geophysical Research*, 101, 3361–3386.
- Koons, P.O. (1989). The topographic evolution of collisional mountain belts: a numerical look at the Southern Alps, New Zealand. *American Journal of Science*, 289, 1041–1069.
- Koons, P.O. (1994). Three-dimensional critical wedges: tectonics and topography in oblique collisional orogens. *Journal of Geophysical Research*, 99, 12301–12315.
- Koons, P.O., (1995). Modeling the topographic evolution of collisional belts. *Annual Review of Earth Planetary Science* 23, 375–408.
- Lane, S.N., and K.S., Richards, (1998). Two-dimensional modelling of flow processes in a multi-thread channel. *Hydrological Processes*, 12, 1279–1298.
- Langendoen, E.J. (2000). CONCEPTS - CONservation Channel Evolution and Pollutant Transport System. *Research Report 16. USDA-ARS-NSL, Oxford, Mississippi*.
- Larsen, I. J. ,and D. R., Montgomery (2012). Landslide erosion coupled with tectonics and river incision *Nature Geoscience*, 5, 468–473.
- Li, M.Z., and C.L., Amos (2001). SEDTRANS96: the upgraded and better calibrated sediment-transport model for continental shelves. *Computers & Geosciences*, 27, 619–645.
- McCuen, R.H. (1998). Hydrologic Analysis and Design. 2nd Ed., Prentice Hall, Upper Saddle River, NJ.
- Mitasova, H., and L. Mitas (1993). Interpolation by regularized spline with tension: I. Theory and implementation. *Mathematical Geology*, 25, 641–655.

- Mitas, L., and H., Mitasova (1998). In: *Modelling Soil Erosion, Sediment Transport and Closely Related Hydrological Processes*, W.Summer, E. Klaghofer and W. Zhang (eds.), IAHS, 249, 81.
- Mitasova, H., C., Thaxton, J., Hofierka, R., McLaughlin, A., Moore, and L., Mitas (2004). Path sampling method for modeling overland water flow, sediment transport and short term terrain evolution in Open Source GIS. in: C.T. Miller, M.W. Farthing, V.G. Gray, G.F. Pinder eds., *Proceedings of the XVth International Conference on Computational Methods in Water Resources*, 1479–1490.
- Montgomery, D. R. (2001). Slope distributions, threshold hillslopes, and steady-state topography. *American Journal of Science*, 301(4-5), 432–454.
- Nikora, V., H., Habersack, T., Huber, and I. McEwan (2002). On bed particle diffusion in gravel bed flows under weak bed load transport. *Water Resource Research*, 38 (6).
- Paik, K. (2008). Global search algorithm for nondispersive flow path extraction. *Journal of Geophysical Research*, 113, 9.
- Paola, C. (2000). Quantitative models of sedimentary basin filling. *Sedimentology*, 47, 121–178.
- Paola, C., and V.R., Voller (2005). A generalized Exner equation for sediment mass balance. *Journal of Geophysical Research*, 110, F4014.
- Paola, C., K. Straub, D. Mohrig, and L. Reinhardt (2009), The "unreasonable effectiveness" of stratigraphic and geomorphic experiments. *Earth-Science Reviews*, 97 (1-4), 1–43.
- Petit, C., Y. Gunnell, N. Gonga-Saholiariliva, B. Meyer, B., and J. Sguinot (2009). Faceted spurs at normal fault scarps: Insights from numerical modeling. *Journal of Geophysical Research*, 114(B5), B05403.
- Planchon, O., and F., Darboux (2001). A fast, simple and versatile algorithm to fill the depressions of digital elevation models. *Catena*, 46, 159–176.
- Press, W., S. Teukolsky, W. Vetterling, and B. Flannery (2007). Numerical Recipes: The Art of Scientific Computing (3rd ed.). New York: Cambridge University Press.
- Qin, C.Z. A.-X. Zhu, T. Pei, B.L. Li, C. Zhou, and L. Yang (2007). An adaptive approach to selecting a flow-partition exponent for a multiple-flow-direction algorithm. *International Journal of Geographical Information Science*, 21 (4), 443–458.
- Quinn, P.F., K.J., Beven, P., Chevallier, and O., Planchon (1991). The prediction of hillslope flow paths for distributed hydrological modeling using digital terrain models. *Hydrological Processes*, 5 (1), 59–79.
- Rickenmann, D. (1999). Empirical relationships for debris flows. *Natural Hazards*, 19, 47–77.
- Rickenmann, D., and M., Zimmermann (1993). The 1987 debris flows in Switzerland: documentation and analysis. *Geomorphology*, 8, 175–189.
- Rosgen, D.L. (2001). A Hierarchical River Stability Watershed-based Sediment Assessment Methodology. *7th Federal Interagency Sedimentation Conference*.
- Rosgen, D.L. (2003). A Critical Review of Stream Classification. *Ph.D. Dissertation, Univ. East Anglia, Norwich, England*.

- Sassa, K. (1988). Geotechnical model for the motion of landslides. *in: Proceedings of the 5th International Symposium on Landslides, 10–15 July, Lausanne, Switzerland*, 3755.
- Scharf, T. E., A. T., Codilean, M., De Wit, J. D., Jansen, and P. W. Kubik (2013). Strong rocks sustain ancient postorogenic topography in southern Africa. *Geology*, 41(3), 331–334.
- Shewchuk, J. (2001). Delaunay refinement algorithms for triangular mesh generation. *Computational Geometry: Theory and Applications*, 22, 1–3.
- Simpson, G., and F. Schlenegger (2003). Topographic evolution and morphology f surfaces evolving in response to coupled fluvial and hillslope sediment transport. *Journal of Geophysical Research*, 108 (B6), 2003.
- Sukumar, N. (2003). Voronoi cell finite difference method for the diffusion operator on arbitrary unstructured grid. *International Journal for Numerical Methods in Engineering*, 57, 1–34.
- Takahashi T. (1981). Estimation of potential debris flows and their hazardous zones : soft countermeasures for a disaster. *Natural Disaster Science*, 3 (1), 57–89.
- Tannehill, J.C., D.A., Anderson, and R.H., Pletcher (1997). Computational fluid mechanics and heat transfer, Second Edition. *Taylor & Francis, Philadelphia*.
- Tarboton, D.G. (1997). A new method for the determination of flow directions and contributing areas in grid digital elevation models. *Water Resources Research*, 33 (2), 309–319.
- Tetzlaff, D., and J. Harbaugh (1989). Simulating clastic sedimentation. *Van Nostrand Reinhold, New-York*.
- Tetzlaff, D., and M.-T. Schafmeister (2007). Interaction among sedimentation, compaction, and groundwater flow in coastal settings. *Geological Society of America Special Papers*, 426, 65–87.
- Thomas, R., S. Lane, and J., Best (2006). A multidimensional marker-in-cell hydraulic and sediment transport model for braided river flow. *proceedings of the Eighth Federal Interagency Sedimentation Conference*, 426, 858–863.
- Tucker, G. E., and R. L., Slingerland (1994). Erosional dynamics, flexural isostasy, and long-lived escarpments: A numerical modeling study. *Journal of Geophysical Research: Solid Earth* (1978–2012), 99(B6), 12229–12243.
- Tucker, G. E., and R. L., Bras (1998). Hillslope processes, drainage density, and landscape morphology. *Water Resources Research*, 34(10), 2751–2764.
- Tucker, G. E., S. T. Lancaster, N. M. Gasparini, R. L. Bras, and S. M. Rybarczyk (2001). An object-oriented framework for distributed hydrologic and geomorphic modeling using triangulated irregular networks. *Computers and Geosciences*, 27, 959–973.
- Tucker, G., and, G., Hancock (2010). Modelling landscape evolution. *Earth Surface Processes and Landforms*, 35, 28–50.
- Vreugdenhill, C.B. (1994). Numerical methods for shallow water flow. *Kluwer Academic, Dordrecht*.
- Warner, J., C., Sherwood, R., Signell, C., Harris, and H., Arango (2008). Development of a three-dimensional, regional, coupled wave, current, and sediment-transport model. *Computers & Geosciences*, 34, 1284–1306.

- Westerink, J.J. (2003). CE 344 Hydraulics Course Notes, Spring 2003. *Department of Civil Engineering and Geological Sciences, University of Notre Dame, Notre Dame*.
- Willgoose, G. (1994). A statistic for testing the elevation characteristics of landscape simulation models. *Journal of Geophysical Research: Solid Earth* (19782012), 99(B7), 13987–13996.
- Willgoose, G. (2005). Mathematical modeling of whole-landscape evolution. *Annual Review of Earth and Planetary Sciences*, 33, 443–459.
- Wohl, E., P.L., Angermeier, B., Bledsoe, G.M., Kondolf, L., MacDonnell, D.M., Merritt, M.A., Palmer, N.L., Poff, and D. Tarboton (2005). River Restoration. *Water Resource Research*, 41.
- Wood, J. (1996). The geomorphological characterisation of digital elevation models. *PhD Thesis, Department of Geography, Univeristy of Leicester, U.K.*, <http://www.soi.city.ac.uk/~jwo/phd>
- Wu, W., Wang, S.S.-Y. and Jia, Y., (2000). Nonuniform Sediment Transport in Alluvial Rivers. *Journal Hydraulic Research, IAHR*, 38(6), 427–434.
- Wu W. (2007). Computational River Dynamics. *Taylor and Francis*, 494 pp.
- Yalin, M.S. (1972). Mechanics of Sediment Transport, *Pergamon Press*.
- Yang, C.T. and S., Wan (1991). Comparisons of selected bed-material load formulas. *Journal of Hydraulic Engineering, ASCE*, 117(8), 973–989.
- Yang, S., J. Yu, and Y. Wang (2004). Estimation of diffusion coefficients, lateral shear stress, and velocity in open channels with complex geometry. *Water Resources Research*, 40 (5), 207–217.
- Zhang, R.J. (1989). Sediment dynamics in rivers, *Water Resources Press*.